A fast polygon inflation algorithm to compute the area of feasible solutions for three-component systems. I: Concepts and applications.

Mathias Sawall[a], Christoph Kubis[b], Detlef Selent[b], Armin Börner[b], Klaus Neymeyr[a]

[a] *Universität Rostock, Institut für Mathematik, Ulmenstrasse 69, 18057 Rostock, Germany*
[b] *Leibniz-Institut für Katalyse, Albert-Einstein-Strasse 29a, 18059 Rostock*

Abstract

The multicomponent factorization of multivariate data often results in non-unique solutions. The so-called rotational ambiguity paraphrases the existence of multiple solutions which can be represented by the area of feasible solutions (AFS). The AFS is a bounded set which may consist of isolated subsets. The numerical computation of the AFS is well understood for two-component systems and is an expensive numerical process for three-component systems. In this paper a new fast and accurate algorithm is suggested which is based on the inflation of polygons. Starting with an initial triangle located in a topologically-connected subset of the AFS, an automatic extrusion algorithm is used to form a sequence of growing polygons which approximate the AFS from the interior. The polygon inflation algorithm can be generalized to systems with more than three components. The efficiency of this algorithm is demonstrated for a model problem including noise and a multi-component chemical reaction system. Further, the method is compared with the recent triangle-boundary-enclosing scheme of Golshan, Abdollahi and Maeder (Anal. Chem. 2011, 83, 836–841).

Key words: factor analysis, pure component decomposition, nonnegative matrix factorization, spectral recovery, band boundaries of feasible solutions, polygon inflation.

1. Introduction

The resolution of multicomponent mixtures is a challenge in analytic chemistry which uses for its solution mathematical tools of nonnegative matrix factorizations. We consider the inverse problem to compute from a spectral data matrix on a time $\times$ frequency grid an approximate factorization into a concentration and an absorptivity matrix. These matrices represent the concentration profiles in time and the absorption spectra of the pure components underlying the chemical reaction system. A serious obstacle of a pure component decomposition procedure is the fact that in nearly all cases a continuum of feasible solutions exists. This fact is well-known from the analysis of relatively simple two-component systems published by Lawton and Sylvestre in 1971 [19]. For three-component systems Borgen and Kowalski [5] provided valuable techniques on the pure component recovery which were extended and deepened by Rajkò and István [26] and also by Golshan, Abdollahi and Maeder [10, 11]. Closely related to this is the computation of minimal and maximal band boundaries by Tauler [29]. For general literature on the pure component decomposition see Malinowski [21], Hamilton and Gemperline [14] and Maeder and Neuhold [20].

In this paper the focus is on the numerical approximation of the *area of feasible solutions* (AFS) for three-component systems. The approach by Borgen and Kowalski [5] allows to represents the AFS by a bounded set in a 2D plane. For a three-component system the AFS is expected to consist of at most three separated subsets. Our work is also inspired by the recent work of Golshan, Abdollahi and Maeder [10] in which the boundary of the AFS is covered by a chain of equilateral triangles.

1.1. The new polygon inflation algorithm

Our idea to approximate the AFS of a three-component system is to inflate an initial triangle in the interior of a topologically-connected subset by an adaptive algorithm. The inflation algorithm subdivides the edges of the polygon recursively and adds new vertices which are located on the boundary of the AFS. A local error estimation is used to control the polygon refinement.

...

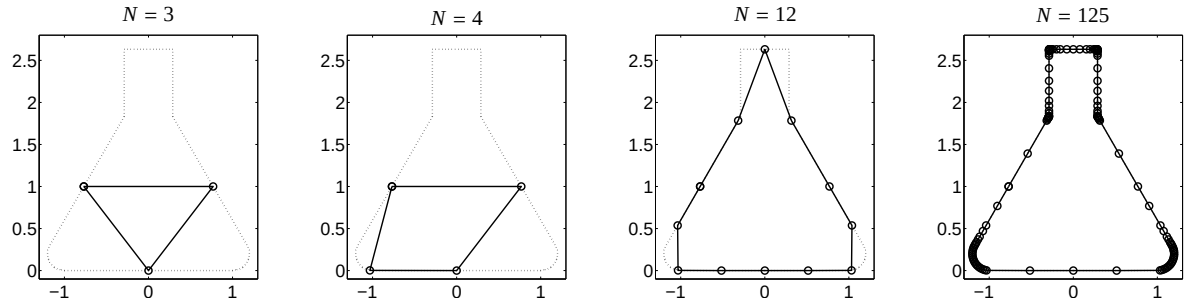

Figure 1: Approximation of the boundary of an Erlenmeyer flask. The initial triangle (left figure) and refined polygons with $N = 4, 12, 125$ vertices are shown. The vertices are computed in an adaptive algorithm in a way that the approximation error is minimized. See Sections 3.4 and 3.5 for the explanation of the parameters ε_b and δ: With $\varepsilon_b = \delta = 10^{-3}$ one gets 125 final vertices, for $\varepsilon_b = \delta = 10^{-4}$ a number of 309 vertices and for $\varepsilon_b = \delta = 10^{-5}$ a number of 781 vertices.

The polygon inflation is illustrated in Figure 1 where the shape of an Erlenmeyer flask, for demonstration purposes, is approximated. A characteristic feature of the algorithm is that it requires only few vertices to approximate straight segments of the boundary. For curved regions the resolution is increased automatically within the adaptive process. The idea of a polygon inflation can be generalized to higher dimensions. A 3D polyhedral construction can be used to treat four-component systems and so on.

1.2. Organization of the paper

Section 2 introduces the Borgen-Kowalski approach for representing the AFS by means of a planar plot for three-component systems. Further, the triangle-boundary-enclosing algorithm from [10] is explained. In Section 3 the new polygon inflation algorithm is presented and its adaptivity and efficiency are discussed. Numerical examples are presented in Sections 4 and 5 where the AFS is computed for the Rhodium-catalyzed hydroformylation. The precision of the algorithm is analyzed under variation of the control parameters and the algorithm is compared with established methods.

2. On the representation of feasible solutions

2.1. The spectral recovery problem

Let $D \in \mathbb{R}^{k\times n}$ be the spectral data matrix which contains in its rows k spectra (taken at k times from a chemical reaction system) and where each spectrum contains absorption values at n frequencies. If the reaction system contains s active species with $s \leq \min(k, n)$, then the concentration matrix $C \in \mathbb{R}^{k\times s}$ contains column-wise the concentration profiles of these species. The absorptivity matrix $A \in \mathbb{R}^{s\times n}$ holds row-wise the spectra of these s species. If nonlinearities and noise are ignored, then the Lambert-Beer law expresses a linear dependence between D, C and A in the form

$$D = CA.$$

The problem of a multivariate curve resolution technique is to find for a given matrix D the correct non-negative matrix factors C and A, see [14, 21]. This is a so-called inverse problem which is ill-posed in the sense that a continuum of possible solutions exists [20]. The following options are available:

1. One can try to recover the desired pure component decomposition by using regularization techniques and/or kinetic models [2, 7, 9, 13, 16, 24, 27]. However, these regularization techniques entail the risk that improper solutions are picked out.
2. In appropriate cases the non-uniqueness can be reduced by a local rank analysis together with an application of the theorems of Manne [22]. Further, partial knowledge of spectra, e.g. of the reactants, or the knowledge of certain concentration profiles allows to apply the complementarity and coupling theorems from [28]. These and other arguments can result in a unique decomposition or at least in some unique factors.
3. If no adscititious information on the reaction system is to be included in the factor analysis, then a computation of the set of all possible solutions appears to be appropriate. See [1, 8, 10, 19, 29] for the AFS for two- and three-component systems.

Here we follow this third and most general approach and aim at a computation of the AFS. Moreover, the AFS can be considered as an own object of research. Numerical methods for its computation appear to be desirable.

2.2. A low-dimensional representation of the AFS

The starting point for the computation of the AFS is a singular value decomposition (SVD) of the spectral data matrix $D \in \mathbb{R}^{k\times n}$. Its SVD reads $D = U\Sigma V^T$ with orthogonal matrices U, V and the diagonal matrix Σ which contains the singular values σ_i on its diagonal. If D is a rank-s matrix, then it holds that $D = U\Sigma V^T = \tilde{U}\tilde{\Sigma}\tilde{V}^T$ with $\tilde{U} = U(:, 1:s) \in \mathbb{R}^{k\times s}$, $\tilde{\Sigma} = \Sigma(1:s, 1:s) \in \mathbb{R}^{s\times s}$ and $\tilde{V} = V(:, 1:s) \in \mathbb{R}^{n\times s}$.

The so-called abstract factors $\tilde{U}\tilde{\Sigma}$ and $\tilde{V}^T$ are usually poor approximations of the matrices C and A. A proper regular transformation by $T \in \mathbb{R}^{s\times s}$ allows to solve the reconstruction problem according to

$$C = \tilde{U}\tilde{\Sigma}T^{-1}, \quad A = T\tilde{V}^T. \tag{1}$$

Any pair of nonnegative matrices $\tilde{U}\tilde{\Sigma}T^{-1}$ and $T\tilde{V}^T$ is called a feasible solution. A feasible solution guarantees a correct reconstruction since $D = (\tilde{U}\tilde{\Sigma}T^{-1})(T\tilde{V}^T)$. However, these factors may have no chemical meaning.

For a two-component system Lawton and Sylvestre [19] have represented the range of feasible solutions. For a three-component system the situation is more complicated but the purpose is still the same. All regular matrices T are to be found so that C and A in (1) are nonnegative matrices. The coefficients of T are the key for a low-dimensional representation of the AFS, see the seminal work of Borgen and Kowalski [5], the important contributions [4, 8, 26, 25] as well as the recent paper [10]. The approach is explained next.

The Perron-Frobenius theory [23] guarantees that the first singular vector $V(:, 1)$ of V can be assumed to be a component-wise nonnegative vector; possibly a multiplication with -1 is to be applied to give a component-wise non-positive vector the desired orientation. With (1) the ith pure component spectrum $A(i, :)$, $i = 1, 2, 3$, reads

$$A(i, :) = t_{i1}V(:, 1)^T + t_{i2}V(:, 2)^T + t_{i3}V(:, 3)^T. \tag{2}$$

Since $V(:, 1) \neq 0$ these spectra can be scaled so that $t_{i1} = 1$ for $i = 1, 2, 3$. Then T has still six degrees of freedom namely t_{i2} and t_{i3} with $i = 1, 2, 3$. The problem is forced to two dimensions by looking only for those $\alpha := t_{12}$ and $\beta := t_{13}$ so that

$$T = \begin{pmatrix} 1 & \alpha & \beta \\ 1 & s_{11} & s_{12} \\ 1 & s_{21} & s_{22} \end{pmatrix}. \tag{3}$$

for proper s_{11}, s_{12}, s_{21} and s_{22} results in a feasible solution.

A point $(\alpha, \beta) \in \mathbb{R}^2$ is called *valid* if and only if there exists at least one regular matrix

$$S = \begin{pmatrix} s_{11} & s_{12} \\ s_{21} & s_{22} \end{pmatrix} \in \mathbb{R}^{2\times 2}, \tag{4}$$

so that T is invertible and both $A = T\tilde{V}^T$ and $C = \tilde{U}\tilde{\Sigma}T^{-1}$ are nonnegative matrices. Hence the AFS can be expressed as the set

$$\mathcal{M} = \left\{(\alpha, \beta) \in \mathbb{R}^2 : \ \mathrm{rank}(T) = 3, \ C, A \geq 0\right\}. \tag{5}$$

Under some mild assumptions the set $\mathcal{M}$ is bounded.

The rows of S and α, β are coupled in the following sense: If $(\alpha, \beta) \in \mathcal{M}$, then the rows $S(i, :)$, $i = 1, 2$, of S are also contained in $\mathcal{M}$. The reason is that an orthogonal permutation matrix $P \in \mathbb{R}^{3\times 3}$ can be inserted in the admissible factorization

$$D = CA = \tilde{U}\tilde{\Sigma}T^{-1}T\tilde{V}^T = (\tilde{U}\tilde{\Sigma}\underbrace{T^{-1}P^T}_{(PT)^{-1}})(PT\tilde{V}^T).$$

The permutation of the rows of T is accompanied with the associated permutation of the columns of T^{-1} and the nonnegativity of the factors is preserved. Further PT and $T^{-1}P^T = (PT)^{-1}$ are a pair of transformation matrices with permuted rows/columns in a way that (s_{i1}, s_{i2}) can substitute (α, β) and vice versa.

2.3. The triangle-boundary-enclosing approach of Golshan, Abdollahi and Maeder

In 2011 Golshan, Abdollahi and Maeder [10] introduced a new approach for the numerical approximation of the boundary of the AFS. This technique is based on an inclusion of the boundary by small equilateral triangles. The algorithm constructs in an initialization phase a first triangle which has at least one vertex in the interior of $\mathcal{M}$ and has also at least one vertex which is not in $\mathcal{M}$. Thus the boundary of the AFS has a nonempty intersection with $\mathcal{M}$. Next this triangle is reflected along one of its edges in a way that the new triangle has once again a vertex in and a vertex not in $\mathcal{M}$. This procedure is continued until the band of triangles includes the entire boundary of a connected subset of the AFS, see Figure 2. The accuracy of this triangle-boundary-enclosing approach depends on the edge length of the triangles. For smaller triangles the accuracy of the boundary approximation increases together with total number of triangles which are used to cover the boundary.

3. The polygon inflation algorithm

The geometric idea of the polygon inflation algorithm is introduced in Section 1.1. Next we describe the algorithm and its mathematical fundamentals.

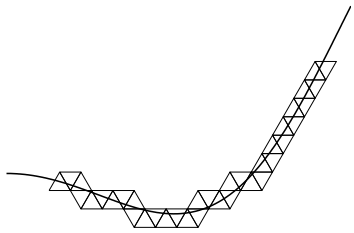

Figure 2: Enclosure of a boundary segment by a chain of equilateral triangles.

3.1. The target function for approximating the AFS

For the computation of the AFS a procedure to classify points $(\alpha,\beta) \in \mathbb{R}^2$ as *valid*, if $(\alpha,\beta) \in \mathcal{M}$, or as *non-valid* in the other case. A procedure for this classification is developed next. Let $\varepsilon \geq 0$ be a small nonnegative real number. Then $-\varepsilon$ is used as a lower bound for the acceptable relative negativeness of the factors C and A in the following way

$$\frac{\min_j C_{ji}}{\max_j |C_{ji}|} \geq -\varepsilon, \quad \frac{\min_j A_{ij}}{\max_j |A_{ij}|} \geq -\varepsilon, \quad i = 1,2,3. \tag{6}$$

The acceptance of small negative components of C and A allows to stabilize the computational process in the case of noisy data.

Let f be a target function which depends on the six degrees of freedom being α, β and $S \in \mathbb{R}^{2\times 2}$, see (3) and (4), so that

$$f : \mathbb{R} \times \mathbb{R} \times \mathbb{R}^{2\times 2} \to \mathbb{R}$$

with

$$\begin{aligned} f(\alpha,\beta,S) = &\sum_{i=1}^{3}\sum_{j=1}^{k} \min(0, \frac{C_{ji}}{\|C(:,i)\|_\infty} + \varepsilon)^2 \\ &+ \sum_{i=1}^{3}\sum_{j=1}^{n} \min(0, \frac{A_{ij}}{\|A(i,:)\|_\infty} + \varepsilon)^2 \\ &+ \|I_3 - TT^+\|_F^2. \end{aligned} \tag{7}$$

Therein C and A are formed according to (1), $I_3 \in \mathbb{R}^{3\times 3}$ is the 3×3 identity matrix, $\|\cdot\|_\infty$ is the maximum vector norm and $\|\cdot\|_F$ is the Frobenius matrix norm [12]. Further T^+ is the pseudo-inverse of T. The last summand $\|I_3 - TT^+\|_F^2$ equals zero if T is an invertible matrix and is positive if T is singular; therefore $f = 0$ guarantees a regular T. The function f is used to form F as follows

$$F : \mathbb{R}^2 \to \mathbb{R}, \quad F(\alpha,\beta) = \min_{S\in\mathbb{R}^{2\times 2}} f(\alpha,\beta,S). \tag{8}$$

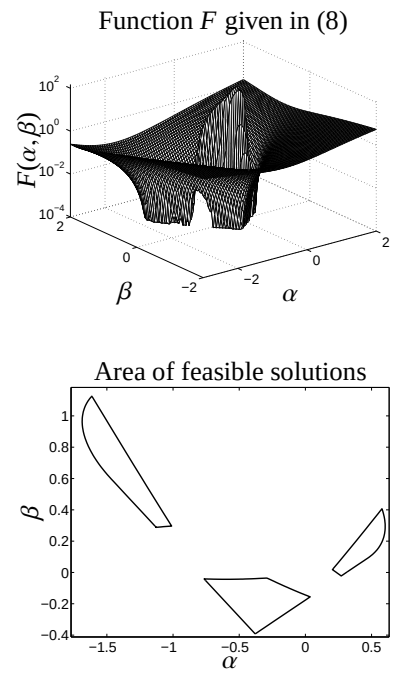

Figure 3: The AFS for the model problem from Section 4. Top: $F(\alpha,\beta)$ on $(\alpha,\beta) \in [-2,2]\times[-2,2]$. Bottom: The AFS with $\varepsilon_b = 10^{-4}$, see (11).

Computationally a point (α,β) is considered as valid if and only if $F(\alpha,\beta) \leq \varepsilon_{\text{tol}}$ with $\varepsilon_{\text{tol}} = 10^{-10}$. Hence,

$$\mathcal{M} = \left\{(\alpha,\beta) \in \mathbb{R}^2 : \; F(\alpha,\beta) \leq \varepsilon_{\text{tol}}\right\}. \tag{9}$$

Figure 3 illustrates F for the model problem which is presented in Section 4 on the domain $(\alpha,\beta) \in [-2,2] \times [-2,2]$.

The evaluation of F requires the solution of a least-squares problem within 4 parameters and with $3(k + n + 3)$ variables. Our function F given in (8) is somewhat different from the pure sum of squares ssq $= \|D - C_+A_+\|_F^2$ as used in [1, 10, 30]; therein C_+ and A_+ are derived from C and A by removing any negative entries. However, we prefer to use (8) for the reason of its numerical stability and as (8) requires a minimization of a sum of only $O(k + n)$ squares. In contrast to this, the minimization of ssq includes the much larger number of $O(k \cdot n)$ summands of squares. Here, the number of components is fixed to $s = 3$. If the approach is generalized to larger s, then the computational costs increase linearly in s.

3.2. Orientation of the AFS

The orientation of the AFS $\mathcal{M}$ depends on the orientation of the singular vectors. The orientation of a

singular vector means that the sign of a singular vector is not uniquely determined in the sense that the simultaneous multiplication of the ith left singular vector and the ith right singular vector with -1 does not change the product $U\Sigma V^T$. However, the orientation of the first left singular vector and the first right singular vector can be fixed in advance by the Perron-Frobenius theory as these two vectors are sign-constant and can therefore be assumed in a component-wise nonnegative form. In other words the SVD $U\Sigma V^T$ with $U \in \mathbb{R}^{k\times 3}$, $V \in \mathbb{R}^{n\times 3}$ is equivalent to the SVD $\hat{U}\Sigma\hat{V}^T$ with

$$\hat{U}(:,1:3) = U(:,1:3)\cdot \mathrm{diag}(1,p_1,p_2),$$
$$\hat{V}(:,1:3) = V(:,1:3)\cdot \mathrm{diag}(1,p_1,p_2)$$

and $p_1, p_2 \in \{-1, 1\}$. The signs of p_i are associated with a reflection of the AFS along the α- or the β-axes.

3.3. Initialization: Generation of a first triangle

Here we refer to the typical case that the AFS consists of three separated subsets. However, the algorithm can also be applied to all other cases. Further the AFS is assumed to be a bounded set; we plan to give a formal proof for this fact in a forthcoming paper. Here the AFS $\mathcal{M}$ is related to feasible matrices representing the pure component spectra. If the AFS for the concentration factor C is of interest, then the whole procedure can be applied to the transposed data matrix D^T.

The algorithm starts with the construction of an initial triangle which is a first coarse approximation of a topologically-connected subset of the AFS. Therefore an admissible factorization $D = CA$ with nonnegative factors C and A is needed. This factorization can be computed by any nonnegative matrix factorization tool [17]. According to (2) the first row $A(1,:)$ reads

$$A(1,:) = V(:,1)^T + \alpha^{(0)}V(:,2)^T + \beta^{(0)}V(:,3)^T.$$

Hence $(\alpha^{(0)},\beta^{(0)}) \in \mathcal{M}$ are determined by

$$T(1,:) = (t_{11}, t_{12}, t_{13}) = A(1,:)\cdot V$$

and

$$\alpha^{(0)} = \frac{t_{12}}{t_{11}}, \quad \beta^{(0)} = \frac{t_{13}}{t_{11}}.$$

This interior point $(\alpha^{(0)},\beta^{(0)})$ is the basis for the construction of the three vertices P_1, P_2, P_3 of the initial triangle on the boundary $\partial\mathcal{M}$ of $\mathcal{M}$. Since $\mathcal{M}$ is a bounded set, P_1 and P_2 can be determined on the straight line along the α-axis through $(\alpha^{(0)},\beta^{(0)})$ having the form

$$x = \begin{pmatrix} \alpha^{(0)} \\ \beta^{(0)} \end{pmatrix} + \gamma \begin{pmatrix} 1 \\ 0 \end{pmatrix}.$$

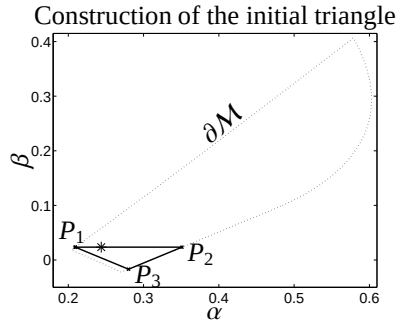

Figure 4: Computation of an initial triangle in $\mathcal{M}$. Dotted line: Boundary of a subset of $\mathcal{M}$. Bold line: the initial triangle. Asterisk: Initial point $(\alpha^{(0)},\beta^{(0)}) = (0.2438,\ 0.0235)$.

Hence $\gamma \geq 0$ for P_1 and $\gamma \leq 0$ for P_2, see Figure 4 for the construction. Then P_3 is one point of intersection of the mid-perpendicular of the line segment $\overline{P_1P_2}$ having the form

$$x = M + \widetilde{\gamma}\upsilon, \quad M = \frac{1}{2}(P_1 + P_2), \quad \upsilon \perp \overline{P_1P_2}.$$

Without loss of generality $\widetilde{\gamma} \leq 0$ can be assumed, see Figure 4.

3.4. The polygon inflation: Adding of vertices

The edges of the initial triangle and also the edges of refined polygons are subdivided by introducing new vertices in a way that the refined polygon is a better approximation of the AFS. Next the adding of a new vertex is explained. Therefore, let the m-gon P with the vertices $(P_1,\ldots,P_m)$ be given. Then P is inflated to an $(m+1)$-gon P' with the vertices $(P'_1,\ldots,P'_{m+1})$. If the edge between P_i and P_{i+1} is selected for the refinement, then the new vertex P'_{i+1} is a point of intersection of the mid-perpendicular of the edge $\overline{P_iP_{i+1}}$ and the boundary $\partial\mathcal{M}$. The refined polygon has the vertices

$$(P'_1, P'_2, \ldots, P'_{m+1}) = (P_1, P_2, \ldots, P_i, P'_{i+1}, P_{i+1}, \ldots, P_m).$$

If P approximates a topologically connected *convex* subset $\mathcal{M}$, then the new vertex P'_{i+1} is located not in the interior of P so that the new polygon P' contains P as a subset. In case of a concave boundary element the new polygon P' may have a smaller area than P. The mid-perpendicular of the edge $\overline{P_iP_{i+1}}$ has the form

$$M + \gamma\upsilon, \quad \gamma \in \mathbb{R} \tag{10}$$

with

$$M = \frac{1}{2}(P_i + P_{i+1}), \quad \upsilon \perp \overline{P_iP_{i+1}}.$$

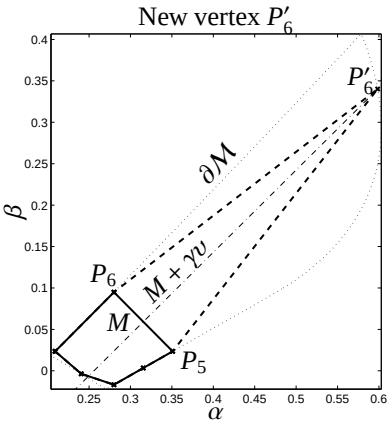

Figure 5: Adding of the vertex P'_6 which is located on the intersection of the mid-perpendicular through P_5 and P_6 and the boundary of $\mathcal{M}$.

The point of intersection of the straight line (10) and $\partial\mathcal{M}$ is not unique (there are two or more points of intersection); the new vertex P'_{i+1} is determined in a way that the Euclidean distance to M is minimized and that the polygon is not dissected into two parts (to avoid to find a new vertex on the opposite side of the polygon, i.e. $\overline{P'_{i+1}M}$ dissects P). Figure 5 illustrates the refinement of a 6-gon to a 7-gon.

The accuracy of a new vertex depends on the function F which is to be minimized along the straight line (10). Numerically we use the relatively slow converging bisection method for the root finding because of its simplicity and robustness. The iteration is stopped if a final accuracy ε_b is reached so that

$$P'_{i+1} \in \mathcal{M}, \qquad \min_{x \notin \mathcal{M}} \left\| P'_{i+1} - x \right\|_2 < \varepsilon_b. \tag{11}$$

The number of iterations depends on ε_b and on the length $\|P_i - P_{i+1}\|_2$ of the edge. In our numerical calculations between 3 iterations (for $\varepsilon_b = 10^{-2}$) and 8 iterations (for $\varepsilon_b = 10^{-5}$) were needed to determine a vertex P'_{i+1}.

3.5. Adaptive edge selection in the refinement process

An adaptive process is used to determine those edges of the polygon whose subdivision promises to improve the approximation of the AFS in the best way. Next a selection strategy is introduced together with a termination criterion.

The central quantity which steers the refinement process is the change-of-area of the polygon which arises if an edge is subdivided. So if an edge $\overline{P_iP_{i+1}}$ is subdivided, then each of the new edges gets a equally weighted gain-of-area

$$\Delta_i = \frac{1}{4} \|P_i - P_{i+1}\|_2 \left\| M - P'_{i+1} \right\|_2 \tag{12}$$

as an attribute. In the next step an edge ℓ is selected for which

$$\ell = \arg\max_j \Delta_j$$

in order to determine an edge which promises a maximal gain-of-area on the basis of its subdivision history. If there is no unique index ℓ, then the algorithm starts with the smallest index. As for the initial triangle no subdivision history is available, all three initial edges are subdivided at the beginning.

The refinement process is stopped if the largest achievable gain-of-area drops below some final accuracy δ. The actual value of δ may depend on the problem. We often use $\delta = \varepsilon_b$.

3.6. Noisy data

The polygon inflation algorithm works well for non-perturbed as well as for noisy data. The parameter ε in (7) controls the allowance of relative negative contributions in C and A and, in our experiments, appears to cause a favorable numerical stability with respect to perturbations.

However, the noise level must be limited in a way that the first three singular vectors $V(:, i)$, $i = 1, 2, 3$, still contain the essential information on the system. If this is not guaranteed, then the expansion (2) cannot guarantee for a proper reconstruction of C and A. Then even no regular transformation T may exist so that C and A are nonnegative matrix factors.

3.7. Efficiency of the polygon inflation

Three characteristic traits of the polygon inflation algorithm are compiled next and are compared with the triangle inclusion method.

1. The polygon inflation algorithm which uses the function (7) has to minimize sums of only $O(k + n)$ squares. In contrast to this the function ssq includes $O(kn)$ squares in [10]. (Note that by the definition of the Landau symbol it holds that $O(k + n) = O(s(k + n))$ where s is the number of components which equals 3 throughout this paper.)
2. Negative entries of C and A larger than $-\varepsilon$ are not completely ignored in the polygon inflation algorithm but affect the minimum of F, see (8). To show that the ssq function from [10] and the function F (8) result in very similar AFSs, we applied

ε	$\mathcal{M}_1$	$\mathcal{M}_2$	$\mathcal{M}_3$
0	0	0	0
$5 \cdot 10^{-3}$	$1.6 \cdot 10^{-4}$	$9.3 \cdot 10^{-5}$	$1.4 \cdot 10^{-4}$
$1 \cdot 10^{-2}$	$5.2 \cdot 10^{-4}$	$2.8 \cdot 10^{-4}$	$4.0 \cdot 10^{-4}$
$5 \cdot 10^{-2}$	$2.1 \cdot 10^{-4}$	$2.2 \cdot 10^{-4}$	$1.5 \cdot 10^{-4}$

Table 1: Comparison of the AFS computed with the function F by (8) and the AFS with ssq according to [10]. The Hausdorff distance of the two AFSs is tabulated for some ε. The accuracy of the boundary approximation is bounded by $\varepsilon_b = 10^{-4}$. Therein $\mathcal{M}_i$ is the ith topologically connected subset of $\mathcal{M}$.

these algorithms to the model problem from Section 4 and used the Hausdorff metric as a measure of distance between these sets. The Hausdorff distance between to sets A and B is

$$\delta(A, B) = \max\left(\max_{a\in A} D(a, B), \max_{b\in B} D(b, A)\right)$$

where $D(x, Y) = \min_{y\in Y}(\|x - y\|_2)$ is the distance of a point x from the set Y. Numerical values of the Hausdorff distances are listed in Table 1; the distances are very small and the sets coincide if $\epsilon = 0$.

3. The polygon inflation algorithm results in a piecewise linear interpolation of the boundary of $\mathcal{M}$ by polygons. The local approximation error of a linear interpolation behaves like $O(h^2)$ if the nodes of the interpolant are assumed to be exact. In contrast to this the enclosure of the boundary by a chain of equilateral triangles with the edge-length h results in a final accuracy which is bounded by the width $O(h)$ of this chain.
   Further, the local adaptivity of the polygon inflation scheme even requires a small number of refinement steps if the boundary is locally more or less a straight line. A critical nonsmooth region of the boundary can be resolved to any desired accuracy. This adaptive resolution of the boundary results in a cost-effective computational procedure. In contrast to this number of triangles needed for the triangle inclusion algorithm increases as $O(1/h)$ in the edge length h of the triangles.

3.8. Selection of parameters

Parameters of the polygon inflation algorithm are:

1. The parameter ε in (6) controls the degree of acceptable negative entries in the columns of C and the rows of A. Negative matrix elements are not penalized in (7) if their relative magnitude is larger than $-\varepsilon$. This parameter should be increased with growing perturbations in the spectral data. In our experience $0 \le \varepsilon \le 0.05$ seems to be working properly. For model problems and in absence of any errors $\varepsilon = 0$ can be used. By construction increasing ε enlarges the AFS.
2. The parameter ε_b in (11) controls the quality of the boundary approximation of the AFS. We used $\varepsilon_b \le 10^{-3}$ and sometimes $\varepsilon_b \le 10^{-4}$. The influence of this parameter on the shape and size of the computed AFS is negligible.
3. The parameter δ defines a stopping criterion for the adaptive polygon refinement. If the largest gain-of -area (12) is smaller than δ, then the refinement can be stopped. We often set $\delta = \varepsilon_b$ and state that the shape and size of the computed AFS is not sensitive for changes of δ.

3.9. Two remarks on the numerical implementation

3.9.1. Numerical optimization

Each step of an iterative minimization of F by (8) includes the solution of a nonlinear optimization problem. For a poorly conditioned problem the numerical solutions will scatter around the exact solution. Hence, a new vertex P'_{i+1} might be located in the interior of the AFS in the following sense

$$\min_{x\notin\mathcal{M}} \left\|P'_{i+1} - x\right\|_2 \ge \varepsilon_b.$$

With such an inaccurate vertex the further refinement steps can result in a nonsmooth boundary which may even contain needles directing towards the inside of the AFS. To avoid such misplaced boundary points, we use the powerful optimization procedure NL2SOL [6] and start the iterative minimization with a good initial guess. A reasonable initial guess can be a convex combination of the numerical solutions which have previously been gained for nearby points. Further, we apply some decision tree before accepting points as valid. Nevertheless, misplaced boundary points can be detected by looking for obtuse angles along the edges of the polygon. Then suspicious vertices may be removed and the optimization can be restarted.

3.9.2. Weakly separated subregions of the AFS

If parts of the boundary of two isolated subregions of the AFS are in close proximity, then the numerical algorithm tends to agglutinate these regions to a joint connected subset. However, for most of the practical problems the subsets of the AFS appear to be well separated.

4. A three-component model problem

Next the polygon inflation algorithm is applied to a three-component model problem. The total computation time and the number of evaluations of points (α, β) concerning their membership in $\mathcal{M}$ is recorded. Further, the accuracy parameters and the noise level are varied. The results are compared with the triangle enclosing algorithm.

4.1. The model problem

We consider the consecutive reactions

$$X \xrightarrow{K_1} Y \xrightarrow{K_2} Z$$

with the vector of kinetic constants $K = (K_1, K_2) = (1, 0.1)$ and with initial concentrations $c(0) = (1, 0, 0)$. Along the time interval $[0, 30]$ a number of $k = 1000$ equidistant nodes is used. The pure component spectra on $[0, 50]$ are set to

$$a_1(\lambda) = \exp(-\frac{\lambda^2}{1000}),$$
$$a_2(\lambda) = \exp(-\frac{(\lambda - 25)^2}{1000}),$$
$$a_3(\lambda) = \exp(-\frac{(\lambda - 50)^2}{1000}).$$

The discretization uses $n = 1500$ equidistant nodes. The resulting spectral data matrix $D \in \mathbb{R}^{1000\times1500}$ is formed according to

$$D_{ij} = C_{i1}A_{1j} + C_{i2}A_{2j} + C_{i3}A_{3j}.$$

Figure 6 shows the factors C and A together with the product matrix D.

4.2. The AFS for C and A

Figure 7 shows the results of a computation of the AFS by means of the polygon inflation algorithm for the concentration factor ($\mathcal{M}_C$) and also for the spectral factor ($\mathcal{M}_A$). The sets $\mathcal{M}_C$ and $\mathcal{M}_A$ are each composed of three isolated and topologically connected subsets. The associated ranges of possible solutions for the concentration profiles are shown in Figure 8. A separate concentration profile is drawn for each vertex of the three polygons which approximate the AFS. Additionally, a concentration profile is drawn for each node of a quadratic mesh which falls into the AFS. One observes that the area (in the sense of an integral) of connected subsets of the AFS is not directly associated with the size of the area which is enclosed by the series of concentration profiles. In other words, a large connected subset of the AFS does not imply strong variations in the associated solutions. This is most evident for the components X and Z (the associated indexes are $i = 1$ and $i = 3$). The variability of the concentration profiles more strongly depends on the variability of the left singular vectors $U(:, i)$, $i = 1, 2, 3$, of D.

4.3. Variation of the accuracy parameters $\varepsilon, \varepsilon_b$ and noisy data

Next a direct comparison is given of the triangle inclusion algorithm [10] with the polygon inflation algorithm from Section 3. Therefore the boundary accuracy parameter ε_b, see (11), is set to $\varepsilon_b = 10^{-2}, 10^{-3}, 10^{-4}$ and the parameter on the acceptance on relative negativeness is set to $\varepsilon = 5 \cdot 10^{-12}$ and $5 \cdot 10^{-3}$, see (6). In our implementation of the triangle inclusion algorithm the parameter ε_b is the side-length of the equilateral triangles. Both $\mathcal{M}_C$ and $\mathcal{M}_A$ are computed and the required number of program calls of F (funcalls) is recorded, see Table 2. Further, the computation time on a standard PC with a 2.4GHz Intel CPU with 16 GB RAM is tabulated. The program code has been written in C and some FORTRAN libraries are used. For the triangle inclusion algorithm the number of funcalls is equal to the number of vertices of the triangles enclosing the boundary of the AFS. In the polygon inflation algorithm multiple funcalls are needed to find a new vertex on the boundary of the AFS by means of the bisection algorithm. However, its total number is always smaller than that for the triangle inclusion approach. If the accuracy parameter ε_b is decreased by one power of 10, then in our implementation of the triangle inclusion scheme the number of funcalls increases with the factor of about 10; in contrast to this the number of funcalls increases with the factor of less than $\sqrt{10}$ for the polygon inflation scheme. All these results appear to be stable if the data are slightly perturbed or if the control parameters for relative negativeness are increased. Figure 9 shows the AFS for the spectral factor A if the control parameters for relative negativeness are set to $\varepsilon \in \{0.05, 0.04, 0.03, 0.02, 0.01, 0\}$.

5. Rhodium-catalyzed hydroformylation

The kinetics of the hydroformylation of 3,3-dimethly-1-butene with a rhodium/tri(2,4-di-*tert*-butylphenyl)phosphite catalyst in *n*-hexane has been studied in detail in [18]. The in situ FTIR spectroscopic data from this publication are reused for a computation of the AFS; for additional information on the reaction conditions and on the experimental HP FTIR apparatus see [18].

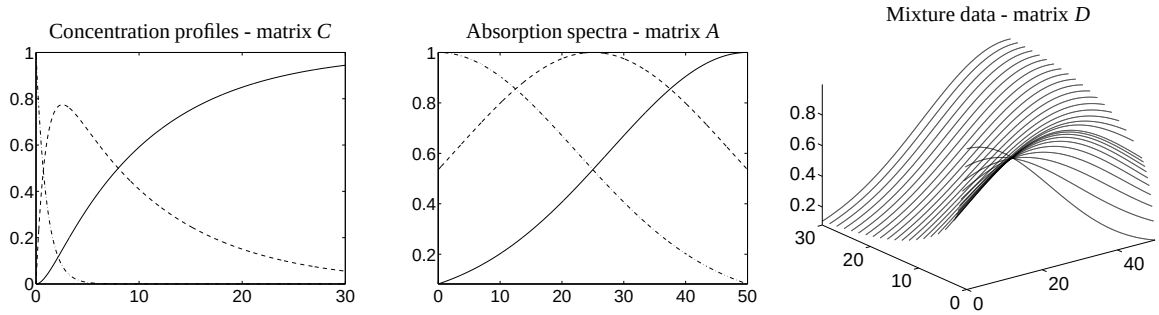

Figure 6: The matrix factors C and A with dash-dotted line for the component X, dashed line for Y and solid line for Z. The right figure shows the product/absorption data D.

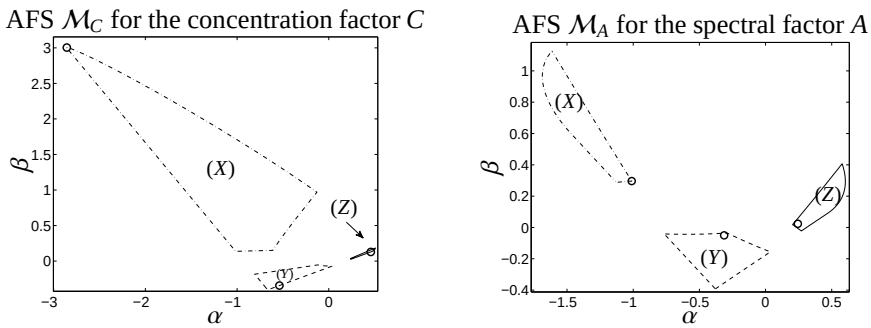

Figure 7: Left: The area of feasible solutions $\mathcal{M}_C$ for the concentration factor C. Right: The area of feasible solutions $\mathcal{M}_A$ for the spectral factor A. For the concentration profiles the solution with the smallest integrated absolute value of the curvature and for which only one reactant is nonzero at time zero have been marked by a small circle. The three associated points in the AFS $\mathcal{M}_A$ are also marked with a circle.

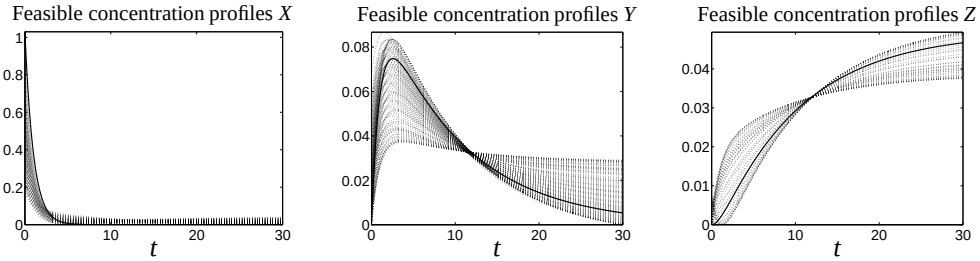

Figure 8: Feasible concentration profiles $C(:, i)$ for the three components $i = 1$ for X, $i = 2$ for Y and $i = 3$ for Z according to the three topologically connected subsets of the AFS $\mathcal{M}_C$ in the left side of Figure 7. The area of a connected subset of the AFS is not correlated with the variability of the range of feasible solutions for the associated component, cf. Section 4.2.

		with $\varepsilon = 10^{-12}$					with $\varepsilon = 5 \cdot 10^{-3}$				
		Triangle inclusion		Polygon inflation			Triangle inclusion		Polygon inflation		
	ε_b	funcalls	time [s]	funcalls	time [s]	vertices	funcalls	time [s]	funcalls	time [s]	vertices
Factor A	10^{-2}	1166	13	352	4	65	1218	13	409	4	81
	10^{-3}	11566	83	1314	12	197	12168	89	1346	11	205
	10^{-4}	115658	660	3413	26	411	121685	685	4001	32	479
factor C	10^{-2}	2334	19	1541	12	81	2733	22	626	7	117
	10^{-3}	23258	153	1966	18	229	27229	178	1666	16	233
	10^{-4}	232477	1341	4465	44	467	272897	1609	4541	44	507

Table 2: The number of program calls of F (funcalls) in order to compute (9) is tabulated for varying ε_b together with the required computing time. The termination is controlled by $\delta = \varepsilon_b$, see Section 3.5. The ratios of required computing time and funcalls is not constant as for computations with higher accuracy better initial values are available. Then convergence can be achieved with only a small number of iterations.

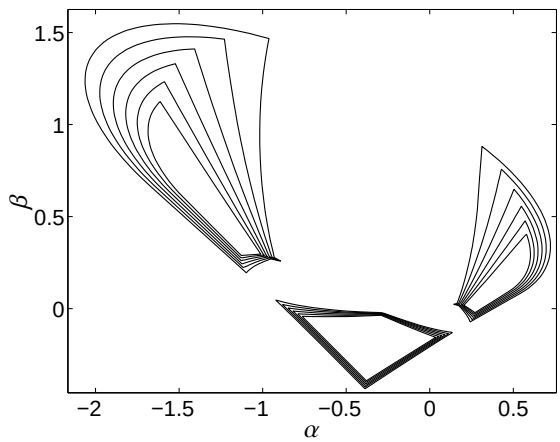

Figure 9: Some different areas of feasible solutions for the factor A for perturbed data and with $\varepsilon \in \{0.05, 0.04, 0.03, 0.02, 0.01, 0\}$.

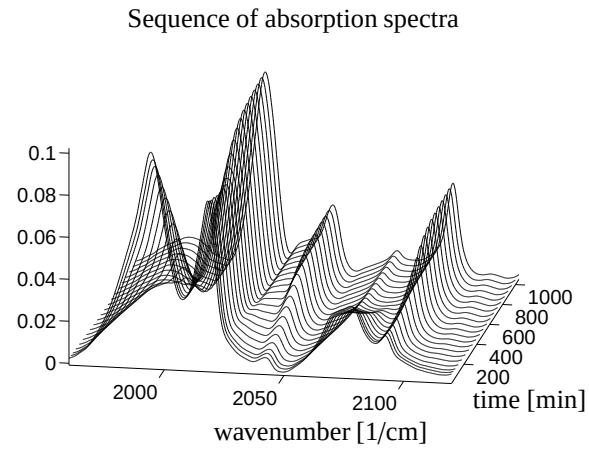

Figure 10: Hydroformylation of 3,3-dimethly-1-butene. Series of FTIR spectra which is determined by three components (olefin, acyl complex and hydrido complex). See Figure 2 in [18] for an assignment of the peaks to the components as well as for the experimental and spectroscopic details.

5.1. The FTIR data

We use a spectroscopic data set which contains characteristic absorptions from three components, namely the olefin, the acyl complex and the hydrido complex. A total number of $k = 1045$ spectra is used and each spectrum contains $n = 664$ spectral channels within the wavenumber interval $[1960, 2120]\text{cm}^{-1}$. The sequence of spectra is shown in Figure 10. The spectroscopic data matrix $D \in \mathbb{R}^{1045\times 664}$ is the basis for the computation of the AFS for a three-component system.

5.2. Computation of the AFS and ranges of feasible solutions

As explained in Section 3.3 a first nonnegative factorization $D = CA$ is to be computed for the initialization. This can be done by standard factorization tools like the PCD code [24] or by the MCR-ANLS algorithm [15], the SPECFIT code [3] or even by the NNMF code [17] written in Matlab. For the given spectroscopic data the permissibility of small negative entries in the factors C and A appears to be important; we use $\varepsilon = 0.01$ in (6). Further, the boundary approximation parameter (11) is set to $\varepsilon_b = 10^{-4}$. The termination parameter is $\delta = 10^{-4}$, see Section 3.5.

Figure 11 shows the two areas of feasible solutions $\mathcal{M}_C$ and $\mathcal{M}_A$. No a priori information has been used for the decomposition, e.g., no mass balance for rhodium is taken into account. The total computation times (the same hardware as in Section 4 is used) are 24.3 seconds for $\mathcal{M}_C$ and 25.0 seconds for $\mathcal{M}_A$. The polygon $\mathcal{M}_C$ is spanned by 479 vertices and 3897 funcalls are needed for its computation; the polygon $\mathcal{M}_A$ contains 417 vertices with 3487 funcalls.

In $\mathcal{M}_A$ only a very small subset, marked by (c), is responsible for the absorption spectrum of the hydrido complex. The corresponding spectrum appears to be nearly unique, see right lower spectrum in Figure 12; an explanation can be derived from the relative concentrations at the end of the reaction and from the isolation of certain peaks in the spectrum of the hydrido complex compared to the spectra of the other components.

This corresponds with a very small range of possible concentration profiles for the olefin, see left upper plot in Figure 12. All other ranges for the concentration profiles and spectra are also shown in Figure 12. As in Section 4.2 a separate concentration profile or spectrum is drawn for each vertex of the AFS. Additionally, a concentration profile or spectrum is plotted for each node of a quadratic mesh which is located in the AFS. Within each plot the smoothest solution with the smallest integral of the absolute value of the discrete second derivative has been plotted by a bold line.

6. Conclusion

A new fast numerical scheme for the adaptive approximation of the AFS for three-component systems by a sequence of polygons has been introduced. Piecewise linear interpolation of the boundary of the AFS results in a local approximation error which behaves like $O(h^2)$ if h is the distance of adjacent vertices. Further, local adaptivity allows to reduce the number of vertices which

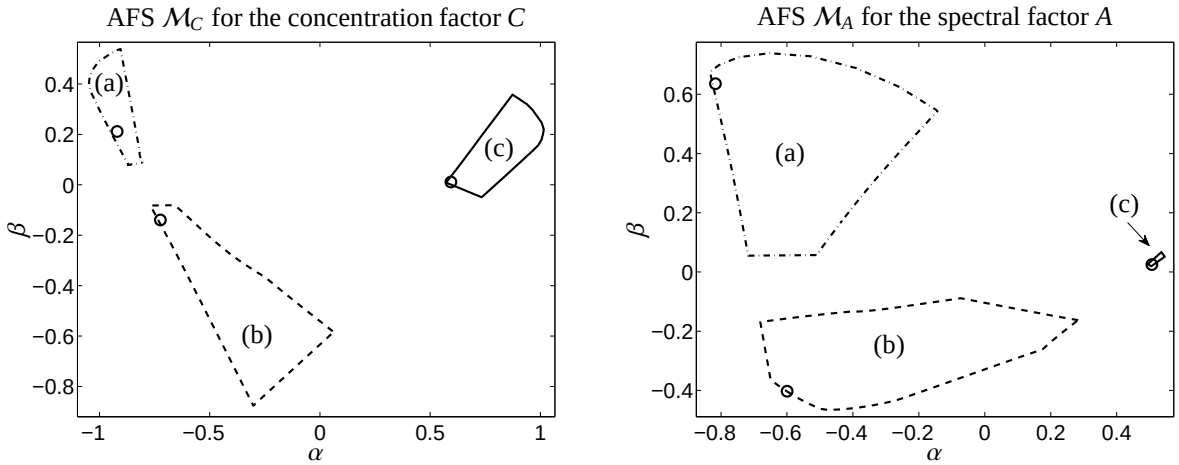

Figure 11: Hydroformylation of 3,3-dimethly-1-butene with an analysis of a three-component subsystem consisting of the olefin, the acyl complex and the hydrido complex. Left: The area of feasible solutions $\mathcal{M}_C$ for the concentration factor. Right: The area of feasible solutions $\mathcal{M}_A$ for the spectral factor.
In $\mathcal{M}_C$ the concentration profiles with the smallest integrated absolute value of the curvature have been marked by a circle. The three associated points in the AFS $\mathcal{M}_A$ are also marked by a circle. Each of three separated subsets of $\mathcal{M}_C$ and $\mathcal{M}_A$ are associated with a specific component. The subset (a) represents the olefin, (b) represents the acyl complex and (c) marks the hydrido complex.

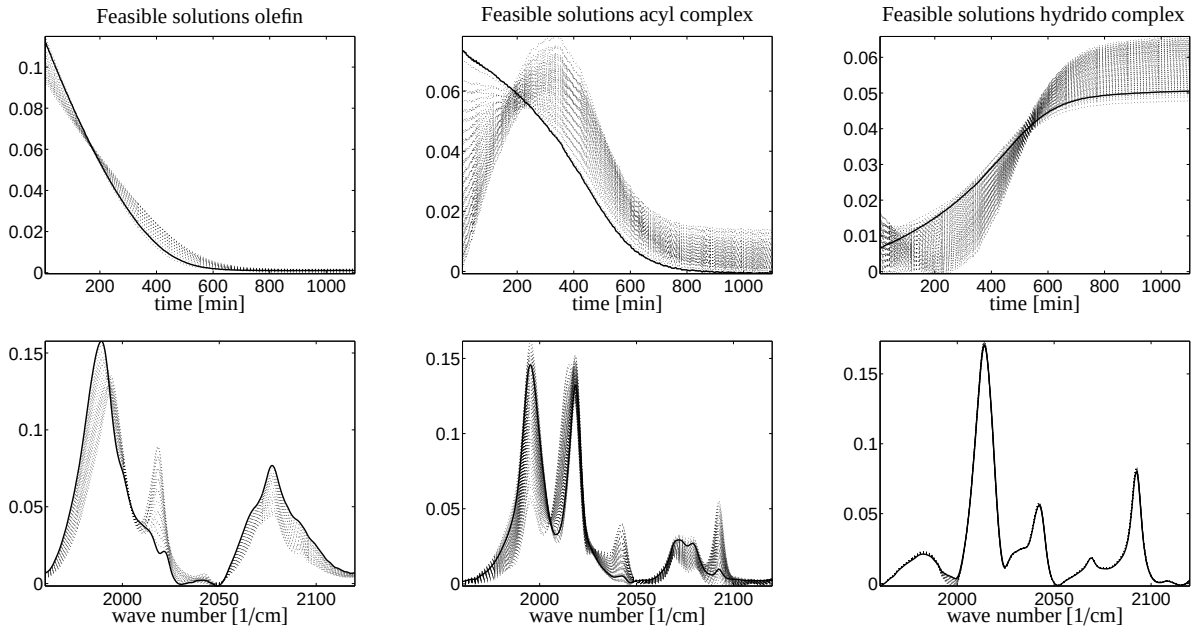

Figure 12: Ranges of the feasible concentration profiles (three upper figures) and ranges of feasible spectra (three lower figures). Left figures: the olefin 3,3-dimethly-1-butene. Middle figures: the acyl complex. Right figures: the hydrido complex. All the ordinates of figures are scaled relatively so that no absolute values on the concentration of absorption should be extracted. No additional information on the reaction system has been used for the decomposition; especially no mass balance on rhodium is taken into account.

are needed to approximate the boundary whenever the boundary is smooth. Numerical calculations show considerable saving in the computation time for the new polygon inflation scheme. For instance for the problem from Section 5 with a 1045×664 data matrix $\mathcal{M}_C$ and $\mathcal{M}_A$ can be computed in only 50 seconds.

The polygon inflation technique can be generalized to a polyhedron inflation scheme in order to approximate the AFS in case of an s-component system with $s \geq 4$. Local adaptive refinement of the faces of the polyhedron can be applied in a way comparable to three-component systems. Finally, we would like to comment that the non-uniqueness of the solutions in an AFS can be reduced if any supplemental information on the system is available; see [28] for some complementarity and coupling theorems.

References

[1] H. Abdollahi, M. Maeder, and R. Tauler. Calculation and Meaning of Feasible Band Boundaries in Multivariate Curve Resolution of a Two-Component System. *Analytical Chemistry*, 81(6):2115–2122, 2009.

[2] M.W. Berry, M. Browne, A.N. Langville, V.P. Pauca, and R.J. Plemmons. Algorithms and applications for approximate nonnegative matrix factorization. *Computational Statistics and Data Analysis*, 52:155–173, 2007.

[3] R.A. Binstead, B. Jung, and A.D. Zuberbühler. SPECFIT/32 Global analysis system. Spectrum Software Associates, Chapel Hill, NC, USA, 2000.

[4] O.S. Borgen, N. Davidsen, Z. Mingyang, and Ø. Øyen. The multivariate N-Component resolution problem with minimum assumptions. *Microchimica Acta*, 89:63–73, 1986. 10.1007/BF01207309.

[5] O.S. Borgen and B.R. Kowalski. An extension of the multivariate component-resolution method to three components. *Analytica Chimica Acta*, 174(0):1–26, 1985.

[6] J. Dennis, D. Gay, and R. Welsch. Algorithm 573: An adaptive nonlinear least-squares algorithm. *ACM Transactions on Mathematical Software*, 7:369–383, 1981.

[7] H. Gampp, M. Maeder, C.J. Meyer, and D. Zuberbühler. Calculation equilibrium constants from multi-wavelength spectroscopy data I, Mathematical considerations. *Talanta*, 32:95–101, 1985.

[8] P.J. Gemperline. Computation of the Range of Feasible Solutions in Self-Modeling Curve Resolution Algorithms. *Analytical Chemistry*, 71(23):5398–5404, 1999.

[9] P.J. Gemperline and E. Cash. Advantages of soft versus hard constraints in self-modeling curve resolution problems. Alternating least squares with penalty functions. *Anal. Chem.*, 75:4236–4243, 2003.

[10] A. Golshan, H. Abdollahi, and M. Maeder. Resolution of Rotational Ambiguity for Three-Component Systems. *Analytical Chemistry*, 83(3):836–841, 2011.

[11] A. Golshan, H. Abdollahi, and M. Maeder. The reduction of rotational ambiguity in soft-modeling by introducing hard models. *Analytica Chimica Acta*, 709(0):32–40, 2012.

[12] G.H. Golub and C.F. Van Loan. *Matrix computations*. Johns Hopkins University Press, Baltimore, MD, third edition, 1996.

[13] H. Haario and V.M. Taavitsainen. Combining soft and hard modelling in chemical kinetics. *Chemometr. Intell. Lab.*, 44:77–98, 1998.

[14] J.C. Hamilton and P.J. Gemperline. Mixture analysis using factor analysis. II: Self-modeling curve resolution. *J. Chemometrics*, 4(1):1–13, 1990.

[15] J. Jaumot and R. Tauler. MCR-BANDS: A user friendly MATLAB program for the evaluation of rotation ambiguities in Multivariate Curve Resolution. *Chemometrics and Intelligent Laboratory Systems*, 103(2):96–107, 2010.

[16] A. Juan, M. Maeder, M. Martínez, and R. Tauler. Combining hard and soft-modelling to solve kinetic problems. *Chemometr. Intell. Lab.*, 54:123–141, 2000.

[17] H. Kim and H. Park. Nonnegative matrix factorization based on alternating nonnegativity constrained least squares and active set method. *SIAM J. Matrix. Anal. Appl.*, 30:713–730, 2008.

[18] C. Kubis, D. Selent, M. Sawall, R. Ludwig, K. Neymeyr, W. Baumann, R. Franke, and A. Börner. Exploring between the extremes: Conversion dependent kinetics of phosphite-modified hydroformylation catalysis. *Chemistry - A Europeen Journal*, 18(28):8780–8794, 2012.

[19] W.H. Lawton and E.A. Sylvestre. Self modelling curve resolution. *Technometrics*, 13:617–633, 1971.

[20] M. Maeder and Y.M. Neuhold. *Practical data analysis in chemistry*. Elsevier, Amsterdam, 2007.

[21] E. Malinowski. *Factor analysis in chemistry*. Wiley, New York, 2002.

[22] R. Manne. On the resolution problem in hyphenated chromatography. *Chemometrics and Intelligent Laboratory Systems*, 27(1):89–94, 1995.

[23] H. Minc. *Nonnegative matrices*. John Wiley & Sons, New York, 1988.

[24] K. Neymeyr, M. Sawall, and D. Hess. Pure component spectral recovery and constrained matrix factorizations: Concepts and applications. *J. Chemometrics*, 24:67–74, 2010.

[25] R. Rajkó. Studies on the adaptability of different Borgen norms applied in self-modeling curve resolution (SMCR) method. *J. Chemometrics*, 23(6):265–274, 2009.

[26] R. Rajkó and K. István. Analytical solution for determining feasible regions of self-modeling curve resolution (SMCR) method based on computational geometry. *J. Chemometrics*, 19(8):448–463, 2005.

[27] M. Sawall, A. Börner, C. Kubis, D. Selent, R. Ludwig, and K. Neymeyr. Model-free multivariate curve resolution combined with model-based kinetics: algorithm and applications. *J. Chemometrics*, 26:538–548, 2012.

[28] M. Sawall, C. Fischer, D. Heller, and K. Neymeyr. Reduction of the rotational ambiguity of curve resolution technqiues under partial knowledge of the factors. Complementarity and coupling theorems. *J. Chemometrics*, 26:526–537, 2012.

[29] R. Tauler. Calculation of maximum and minimum band boundaries of feasible solutions for species profiles obtained by multivariate curve resolution. *J. Chemometrics*, 15(8):627–646, 2001.

[30] M. Vosough, C. Mason, R. Tauler, M. Jalali-Heravi, and M. Maeder. On rotational ambiguity in model-free analyses of multivariate data. *J. Chemometrics*, 20(6-7):302–310, 2006.